Title

3D printed Mg-NiTi interpenetrating-phase composites with high strength, damping capacity, and energy absorption efficiency

Journal

Science Advances, 6(19)

ISSN

2375-2548

Authors

Zhang, Mingyang
Yu, Qin
Liu, Zengqian
et al.

Publication Date

2020-05-08

DOI

10.1126/sciadv.aba5581

Peer reviewed

MATERIALS SCIENCE

3D printed Mg-NiTi interpenetrating-phase composites with high strength, damping capacity, and energy absorption efficiency

Mingyang Zhang[1,2], Qin Yu[3], Zengqian Liu[1,2]*, Jian Zhang[1], Guoqi Tan[1,2], Da Jiao[1], Wenjun Zhu[4], Shujun Li[1]*, Zhefeng Zhang[1,2]*, Rui Yang[1,2], Robert O. Ritchie[3,5]*

It is of significance, but still remains a key challenge, to simultaneously enhance the strength and damping capacities in metals, as these two properties are often mutually exclusive. Here, we provide a multidesign strategy for defeating such a conflict by developing a Mg-NiTi composite with a bicontinuous interpenetrating-phase architecture through infiltration of magnesium melt into three-dimensionally printed Nitinol scaffold. The composite exhibits a unique combination of mechanical properties with improved strengths at ambient to elevated temperatures, remarkable damage tolerance, good damping capacities at differing amplitudes, and exceptional energy absorption efficiency, which is unprecedented for magnesium materials. The shape and strength after deformation can even be largely recovered by heat treatment. This study offers a new perspective for the structural and biomedical applications of magnesium.

INTRODUCTION

Lightweight magnesium and magnesium alloys are distinguishable among metallic materials due to their high specific strength and specific stiffness, i.e., strength and stiffness normalized by density (*1*, *2*). However, their load-bearing applications are limited by their low strengths at both ambient and elevated temperatures and relatively poor ductility as compared to other structural metals, e.g., steels and aluminum alloys. By contrast, magnesium and magnesium alloys exhibit outstanding damping characteristics, which outperform most other metallic materials because of the easy twinning, easy motion of dislocations, and weak dislocation pinning at defects or impurities (*3*, *4*). This makes them promising for applications involving the dissipation of mechanical energy and for reducing vibrations. In this context, it is important to improve the strength of magnesium (and magnesium alloys) without compromising such high damping capacity. However, the strength and damping capacity are often mutually exclusive properties, as common strengthening approaches in magnesium invariably lower the damping capacity (*1*, *2*, *5*–*11*). This is essentially an embodiment of the general trade-off relationship between strength and plasticity in metals (*12*). Such a conflict is also pertinent for magnesium-based composites, which are reinforced by dispersing a second phase in the magnesium matrix. These composites usually exhibit a reduced ductility due to the discontinuous nature of the reinforcement with the resulting local stress concentrations in the matrix (*5*, *9*, *13*–*15*). In addition, as with most engineering materials, the original shape and strength of magnesium alloys and composites can rarely be recovered once inelastic deformation or damage has occurred. It would thus be highly desirable in the quest for enhanced durability if the notion of shape memory or self-recovery could be realized in Mg-based materials, which could further open possibilities for engineering smart versions of these materials and structures with new functionalities.

To address these issues, we propose here a multidesign strategy, which encompasses the deliberate modulation of the phase constitution and architecture of magnesium composites together with the development of feasible fabrication techniques to accomplish it. First, we selected a reinforcing phase to strengthen the magnesium, in the form of the shape-memory Nitinol alloy, which among metals has relatively good damping capacities (*16*). This alloy exhibits an in situ reversible martensite-to-austenite phase transformation at elevated temperatures where the magnesium creeps at minimal stress levels (*16*, *17*); the internal stress produced by this transformation can provide the driving force for the shape recovery of the composite. Second, we designed a three-dimensional (3D) interpenetrating-phase architecture such that the separate constituent phases are topologically bicontinuous and interconnected (*18*, *19*). In this respect, the structural integrity and continuity of the Nitinol alloy are necessary for generating an improved strengthening efficiency and adequate recovery in the composite by promoting effective load transfer. Such a structure may also facilitate the achievement of a sound damping capacity and an enhancement in damage tolerance (*19*, *20*). Third, we used a two-step process of additive manufacturing of a Nitinol scaffold and subsequent pressureless infiltration of the magnesium melt into the scaffold to fabricate the Mg-NiTi composite. Additive manufacturing provides a viable means for controlling the 3D architectures of the Nitinol reinforcement within the final composite. Melt infiltration is enabled by the large temperature gap between the melting points of Nitinol and magnesium (i.e., 1310° and 648°C, respectively) along with their minimal mutual reaction or solubility at moderately higher temperatures than the melting point of magnesium (*21*).

This study presents a proof of concept of how to simultaneously achieve high strength, exceptional damping capacity, good energy absorption efficiency, and a remarkable self-recoverable capability in a Mg-NiTi interpenetrating-phase composite. Our objective

[1]Institute of Metal Research, Chinese Academy of Sciences, Shenyang 110016, China. [2]School of Materials Science and Engineering, University of Science and Technology of China, Hefei 230026, China. [3]Materials Sciences Division, Lawrence Berkeley National Laboratory, Berkeley, CA 94720, USA. [4]National Key Laboratory of Shock Wave and Detonation Physics, Institute of Fluid Physics, Mianyang 621900, China. [5]Department of Materials Science and Engineering, University of California Berkeley, Berkeley, CA 94720, USA.
*Corresponding author. Email: zengqianliu@imr.ac.cn (Z.L.); shjli@imr.ac.cn (S.L.); zhfzhang@imr.ac.cn (Z.Z.); roritchie@lbl.gov (R.O.R.)

resides not only in creating an unprecedented combination of properties in magnesium-based materials, which is appealing for structural and biomedical applications, but also in providing a new design concept and fabrication approaches that could be applicable to engineer other material systems for improved performance.

RESULTS

Formation and microstructure

Figure 1A illustrates the formation process of the Mg-NiTi interpenetrating-phase composite. The controlled architecting of the Nitinol reinforcement in the composite in the form of rhombic dodecahedrons was achieved through 3D printing of the Nitinol scaffold in line with the stereolithographic model. A dense composite was generated by infiltration of the scaffold with the magnesium melt and subsequent solidification. X-ray tomography (XRT) volume renderings of the infiltrated composite (Fig. 1B) reveal a complete filling of the open pores in the scaffold by the magnesium. The spatial distribution of the Nitinol scaffold within the composite, as indicated by the filtered signal by excluding magnesium (Fig. 1C), demonstrates the bicontinuous nature of both constituent phases and their mutual interpenetration in three dimensions. The volume fraction of Nitinol in the composite was determined to be ~35.9% by XRT. The density of the composite was measured to be 3.21 g cm^{-3}; as this conforms to the value calculated from the rule-of-mixtures, this implies that the volume content of unfilled pores was negligible.

Scanning electron microscopy (SEM) micrographs of the Mg-NiTi composite (Fig. 2A) further reveal the absence of obvious structural flaws, e.g., pores or microcracks, in both constituents and at their interfaces. The composite principally comprised magnesium and Nitinol with no evidence of notable amounts of other phases, as shown by the x-ray diffraction (XRD) pattern in the inset. Nevertheless, magnified SEM imaging indicated the emergence of new phases at the interfaces between the two constituents and at the grain boundaries of the magnesium matrix (Fig. 2B). Energy-dispersive x-ray spectroscopy (EDS) measurements showed that the Ti and Ni elements were relatively enriched, respectively, in the interfacial phase between the magnesium and Nitinol and in the intergranular magnesium precipitates (Fig. 2C). The latter phase was determined to be Mg_2Ni by microzone XRD analysis (*21*), as shown in Fig. 2D. Such a redistribution of elements, specifically the deficiency of nickel at the interfacial region between the constituents, is presumed to be caused by the diffusion of Ni atoms from Nitinol into the magnesium to form the Mg_2Ni phase during infiltration.

Ambient-temperature mechanical properties

Figure 3A shows a representative engineering compressive stress-strain curve for the Mg-NiTi interpenetrating-phase composite measured at ambient temperature. The stress-strain curves for pure magnesium, solidified from the infiltration temperature along with the composite, and the 3D printed Nitinol scaffold (without Mg infiltration) are also presented for comparison. The stress in the composite increases after initial yielding at ~80 MPa, before displaying a plateau or slight decrease after reaching a maximum of ~320 MPa and before exhibiting a progressively increasing trend at strains above ~35%. Hence, the composite demonstrates markedly higher stresses, at a specific strain, than for pure magnesium or the Nitinol scaffold, which are well above estimates from the rule-of-mixtures. The successive loading-unloading stress-strain curves for the composite, shown in Fig. 3B, reveal the hysteresis effect as manifested by the detectable circumscribed area in the stress-strain hysteresis loop during each unloading-reloading cycle. This implies that the imposed mechanical energy can be additionally dissipated by mechanisms beyond merely plasticity or damage, in particular, involving internal friction (*22*), in the composite during cyclic loading-unloading conditions.

The variation in the characteristic energies ($E_{consumed}$, $E_{dissipated}$, and $E_{elastic}$) under the curve at each loading cycle, as schematically illustrated in the inset in Fig. 3B, can provide insight into the deformation processes in the composite. As shown in Fig. 3C, the mechanical energy consumed by irreversible deformation ($E_{consumed}$), e.g., plasticity in magnesium and damage in the precipitates, presents an initial increasing trend with loading cycles or applied stress but becomes almost constant at roughly 150 MPa (point A), i.e., 15 cycles, before increasing again. Such a transition is presumed to be caused by global yielding of the Nitinol phase, as subsequent work hardening tends to decrease the plastic deformation in the composite over an equal increase of stress. The elastically restored energy ($E_{elastic}$) and

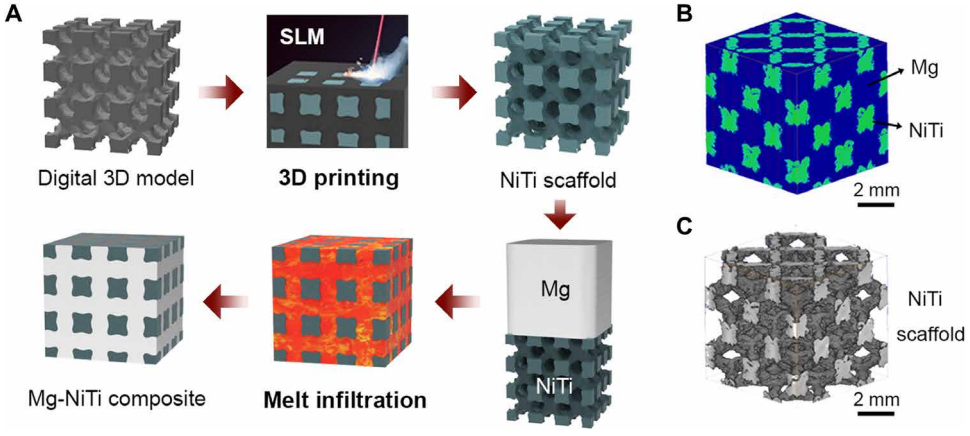

Fig. 1. Formation and 3D architecture of Mg-NiTi interpenetrating-phase composite. (**A**) Schematic illustration of the fabrication process of the Mg-NiTi interpenetrating-phase composite by 3D printing of a Nitinol scaffold and subsequent pressureless infiltration of the scaffold with magnesium melt. SLM, selective laser melting. (**B** and **C**) XRT volume renderings of (B) the infiltrated composite and (C) Nitinol reinforcement in the form of rhombic dodecahedrons within the composite, obtained by filtering out the signal from the magnesium.

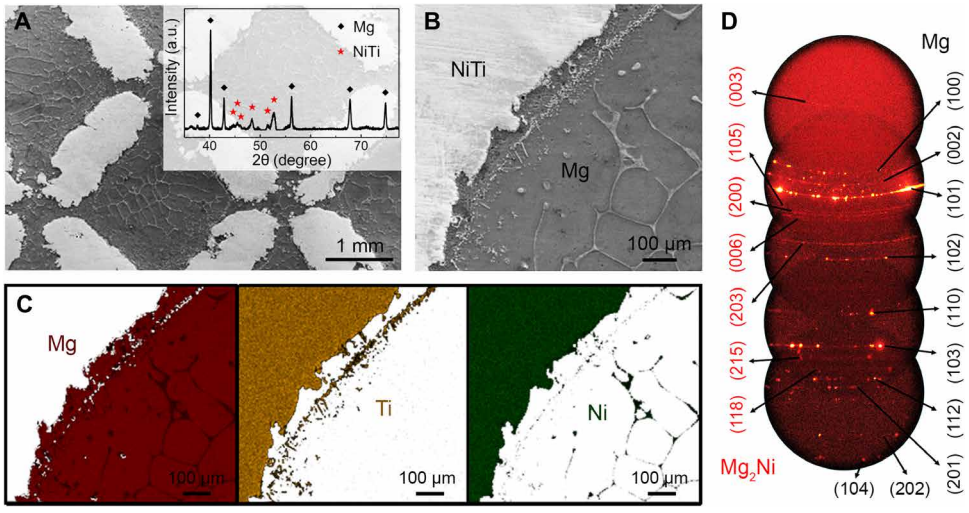

Fig. 2. Microstructure and phase constitution of the Mg-NiTi interpenetrating-phase composite. (**A** and **B**) SEM images of (A) Mg-NiTi composite and (B) magnified micrograph of the interfacial region between the Nitinol and magnesium phases. The inset in (A) shows the XRD pattern of the entire composite. a.u., arbitrary units. (**C**) Area distributions of Mg, Ti, and Ni elements obtained by EDS measurements in the region corresponding to the SEM image in (B). (**D**) Microzone XRD pattern of the precipitates at the grain boundaries of the magnesium matrix. The characteristic diffraction peaks of the crystallographic planes of magnesium and Mg_2Ni phases are indicated in the figure.

viscoelastically dissipated energy ($E_{dissipated}$) display similar variations in the form of a continuous increase to a steady level with a transition point (point B) conforming exactly to the onset of the stress plateau on the monotonic stress-strain curve (Fig. 3A). This is believed to result from the exhaustion of the work-hardening ability and the occurrence of critical damage in the composite, which limit any further increase in strength and internal friction. Hence, the subsequent deformation becomes dominated by the evolution of irreversible damage. The composite exhibits a high energy dissipation ratio, i.e., the proportion of dissipated energy in the total energy, exceeding 24% over a wide range of stress above 80 MPa, as shown in the inset. This implies a good damping capacity of the composite.

Figure 3D presents the variations in true compressive stress and corresponding work-hardening rate, i.e., the derivative of true stress with respect to true strain, as a function of the true strain in the Mg-NiTi composite. The entire deformation process can be divided into five stages. In stage I, both magnesium and Nitinol are principally deformed elastically. The onset of global plastic deformation in the magnesium can be determined from the initial yielding of composite, which occurs at ~80 MPa. After that point, the composite displays a mixed mode of deformation synergized from the plasticity of the magnesium and elasticity in the Nitinol (stage II). Stage III ensues with the yielding of Nitinol at ~150 MPa (point A in Fig. 3C). At this stage, both constituents are plastically deformed and work hardened. The strong hardening behavior of the Nitinol leads to some recovery in the work-hardening rate of the composite. (For comparison, the deformation behavior of 3D printed dense Nitinol, using the same parameters as for the Nitinol scaffold, is shown in fig. S1.) After reaching the stress maximum of ~320 MPa (at a true stress of ~280 MPa), the true stress begins to decrease because of diminished work hardening and the evolution of irreversible damage (stage IV). The large deformation with true strain exceeding ~45% produces a complex stress state and constrained friction at the contact interfaces between the composite and the compressive platens (*18*). This results in the final stage where the true stress displays a slightly increasing trend with strain (stage V).

Damaging process and mechanisms

The Mg-NiTi composite was successively compressed to increasing strains of 2, 5, 10, 15, and 30%, unloaded at each strain, and then examined by SEM to investigate the evolution of damage. Figure 4 (A to E) shows the representative morphologies of the damage, specifically associated with development of cracks in the composite at differing strains during compressive deformation. The damaging process and mechanisms are schematically illustrated in Fig. 4F. Initial damage at 2% strain occurred in the form of intergranular cracking of the magnesium matrix adjacent to the Mg_2Ni precipitates (Fig. 4A). With an increase in strain to 5%, partial separation between the magnesium and Nitinol was apparent at the Ti-rich interfacial phase (Fig. 4B). These results demonstrate a higher tendency of damage associated with the precipitates introduced during melt infiltration process.

As the strain increased to 10% where the stress approached its maximum, microcracks formed in the Nitinol skeleton at locations such as pores, incomplete melt powder inclusions, and regions of inadequate fusion between adjacent layers (Fig. 4C). These defects are not fully understood in terms of their formation mechanisms and are seemingly unavoidable in 3D printed metals (*23*–*25*). The interfacial cracks were seen to invade the Nitinol skeleton and to cause its splitting at 15% strain (Fig. 4D). This deteriorated the continuity and integrity of the Nitinol reinforcement and resulted in a drop in stress on the stress-strain curve (stage IV in Fig. 3D). Further compression to ~30% strain led to the destruction of the Nitinol skeleton, specifically at its nodes, because of the coalescence, linkage, and extension of cracks throughout the struts (Fig. 4E). This was accompanied by substantial plastic deformation of the magnesium matrix; however, the composite still remained intact, owing to its interpenetrating-phase architecture, and retained to a large extent its load-bearing capacity.

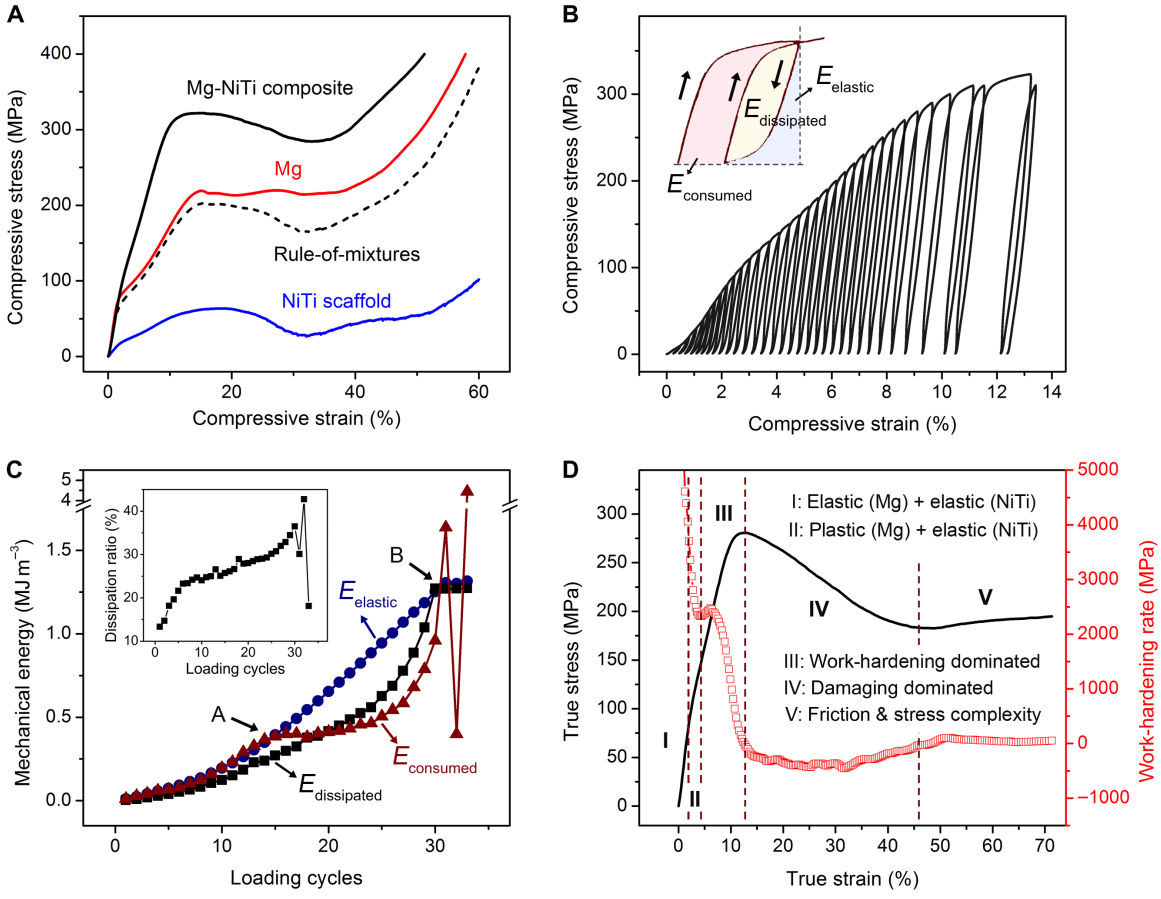

Fig. 3. Ambient-temperature mechanical properties and deformation process of the Mg-NiTi composite. (**A**) Representative engineering compressive stress-strain curve of interpenetrating-phase composite at ambient temperature and its comparison with those of the pure magnesium, Nitinol scaffold, and their combination according to the rule-of-mixtures. (**B**) Cyclic loading-unloading stress-strain curves for the composite up to the stress maximum for monotonic compression. The inset illustrates the characteristic energies under the curves at each loading cycle. (**C**) Variations of specific energies with loading cycles during the cyclic loading-unloading process. A and B denote the transition points, respectively, for the consumed energy by irreversible deformation (A) and for the elastically restored and viscoelastically dissipated energies (B). The inset shows the energy dissipation ratios as a function of the loading cycles. (**D**) Variations in the true compressive stress and nominal work-hardening rate with true strain for the five stages of the deformation process in the composite. It is noted that the general varying trend of work-hardening rate remains constant, although its absolute value may be underestimated because of the difficulty in fully eliminating the deformation from the compressive platens.

High-temperature and dynamic mechanical properties

In addition to the strengthening effect at ambient temperature, the Mg-NiTi interpenetrating-phase composite can sustain markedly higher stresses (at equal strains) than its individual constituents at elevated temperatures of 200° and 350°C; this further applies to the combinations of its constituents according to the rule-of-mixtures (Fig. 5, A and B). With increasing temperature, the strength of pure magnesium is known to markedly decrease, leading to creep deformation at low stress levels. In contrast, the load-bearing capability of Nitinol scaffold is relatively independent of the temperature, remaining essentially constant up to 350°C. Hence, with increasing temperature, the strength of the entire composite, as indicated by the plateau stress (defined in fig. S2), becomes increasingly determined by the Nitinol phase; consequently, it displays far less a deterioration in strength at higher temperatures than pure magnesium. Specifically, the plateau stresses of the composite are more than 200 and 120 MPa at 200° and 350°C, which are respectively ~56 and ~26% higher than those predicted by the rule-of-mixtures. The apparent stress drop in the composite at strains exceeding ~25% strain is presumed to be caused by the global instability or destruction of the Nitinol framework (*22*, *26*, *27*).

Figure 5 (C and D) shows the measured damping properties of the composite, compared to those of the pure magnesium and Nitinol scaffold, at strain amplitudes of 0.001 and 0.1%, representing relatively weak and strong vibrations, respectively, at temperatures from ambient to 350°C. The corresponding damping properties for moderate amplitude of 0.01% are shown in fig. S3. The composite can be seen to exhibit good damping capabilities, as indicated by a high internal friction, Q^{-1}, which is defined using the tangent value of the phase angle between the stress and strain measured by dynamic mechanical analysis (DMA), exceeding 0.02 and 0.08, respectively, at amplitudes of 0.001 and 0.1% at ambient temperature. Specifically, the internal friction was more than 5 and 12 times, respectively, higher than that of pure magnesium and the Nitinol scaffold for strain amplitudes of 0.001% below 100°C, implying a unique potency of the Mg-NiTi composite in minimizing weak vibrations. For strong vibrations, which are more stringent but widespread in practical applications, the composite invariably has better damping capacities

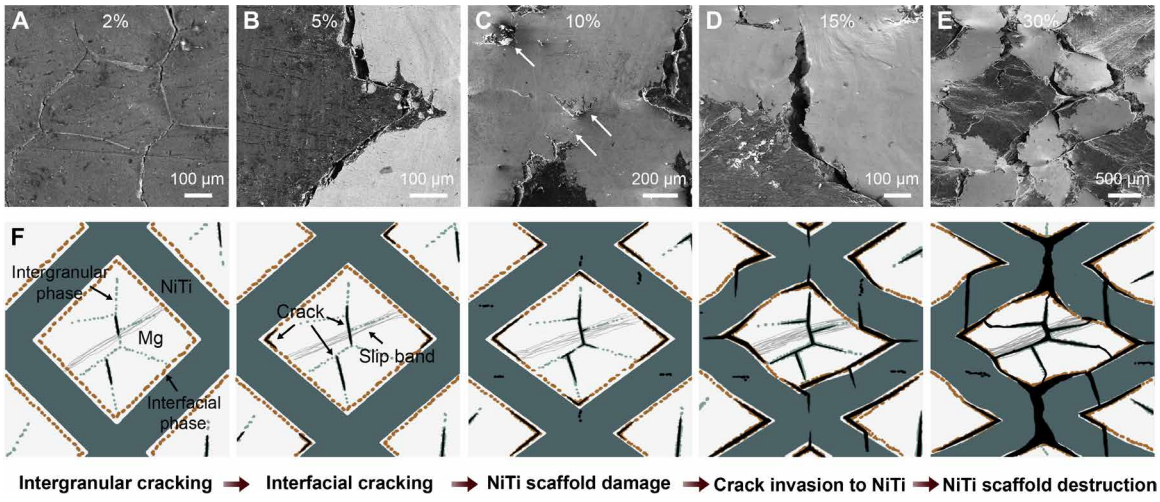

Fig. 4. Mechanisms of damage in the Mg-NiTi interpenetrating-phase composite during deformation. (**A** to **E**) Representative SEM micrographs of damage in the composite at successively increasing engineering compressive strains of (A) 2%, (B) 5%, (C) 10%, (D) 15%, and (E) 30%. The arrows in (C) indicate microcracks that preferentially form at defects in the Nitinol skeleton. (**F**) Schematic illustrations of the damage evolution process in the composite during compressive deformation.

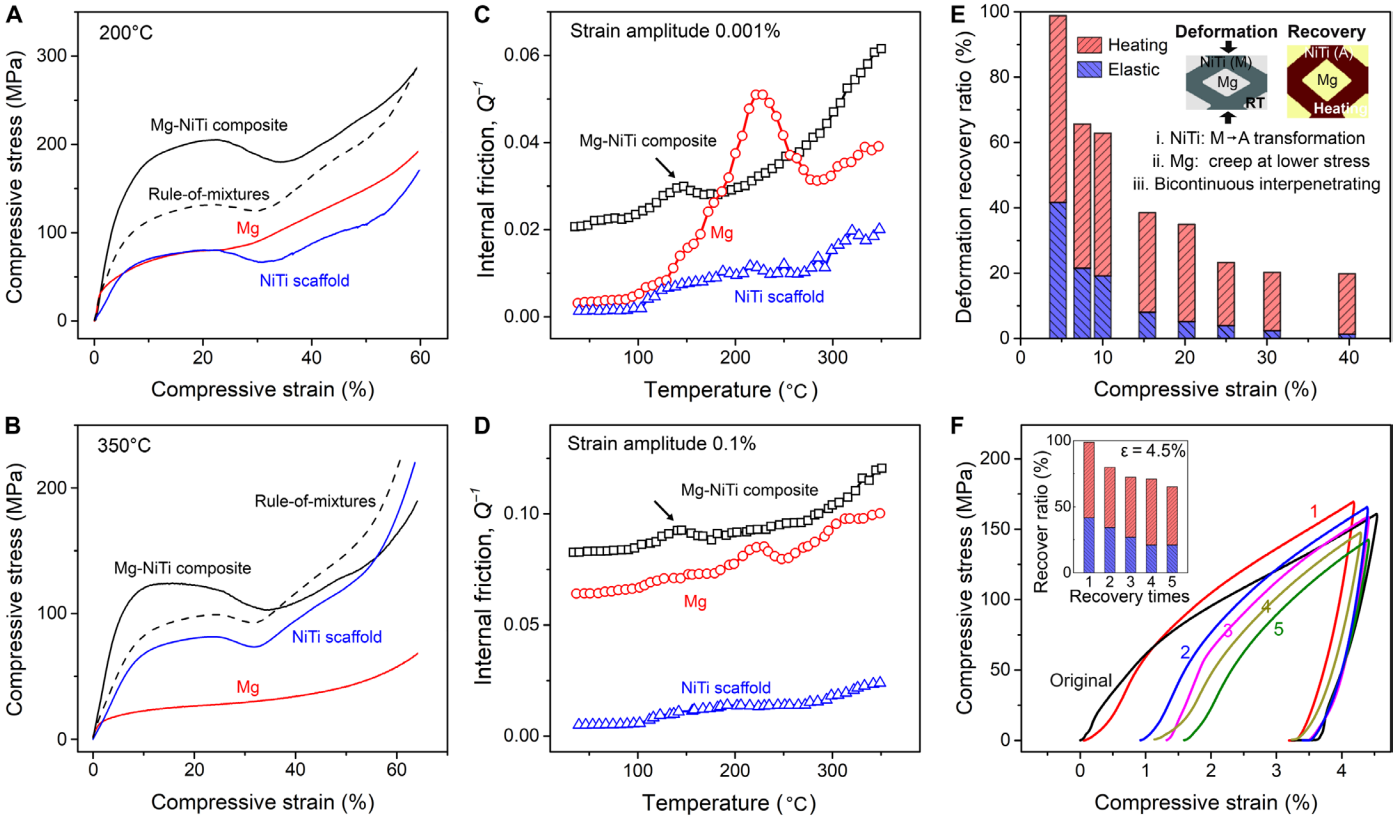

Fig. 5. High-temperature and dynamic mechanical properties of the composite along with its shape recovery behavior. (**A** and **B**) Representative engineering compressive stress-strain curves of the Mg-NiTi composite at (A) 200°C and (B) 350°C, compared with those of pure magnesium, Nitinol scaffold, and their combinations according to the rule-of-mixtures. (**C** and **D**) Variations in the internal friction of the composite from ambient temperature up to 350°C, as measured by DMA at strain amplitudes of (C) 0.001% and (D) 0.1% and a frequency of 1 Hz. The damping properties of pure magnesium and the Nitinol scaffold are also shown for comparison. The arrows indicate the damping extrema of the composite at ~150°C. (**E**) Deformation recovery ratio, i.e., the ratio of recovered to total deformation, in the form of elastic recovery and by heat treatment of the composite at different compressive strains. Vertical columns, with their midpoints along the *x* axis indicating specific strains, are used here for clarity. The conditions and mechanisms for the shape recovery behavior are illustrated in the inset, with the symbols M and A representing martensite and austenite, respectively. (**F**) Compressive stress-strain curves for the composite after it had been repeatedly deformed to ~4.5% strain and then recovered via heat treatment for up to five times. The deformation recovery ratios at each recovery time are given in the inset.

than its constituents over the entire temperature range. The internal friction of the composite displayed a global increasing trend with increasing temperature at both amplitudes, with an extremum at around 150°C, as indicated by the arrows, which may result from the martensite-to-austenite phase transformation of the Nitinol phase (*16*). The internal friction of the Nitinol scaffold also showed a sudden rise at ~110°C, which conforms exactly to the onset of the damping extremum of the composite. The appearance of a damping extremum for pure magnesium at around 230°C, which is particularly noticeable for 0.001% amplitude, is deemed to be caused by the activation of grain boundary sliding (*28*). Such an improved internal friction, accompanied by a simultaneous strengthening effect in the composite, is rarely attainable in traditional magnesium alloys and their composites (*5*–*11*).

Shape recovery behavior

In addition to the synergetic enhancement in both strength and damping capacities, the Mg-NiTi interpenetrating-phase composite is capable of recovering to a large extent its initial shape after deformation. This can be achieved by heating the composite to a temperature range where the Nitinol and magnesium exhibit a martensite-to-austenite phase transformation and creep deformation, respectively [the characteristic temperature range for the phase transformation of Nitinol at heating was measured to be 60° to 100°C by differential scanning calorimetry (DSC), as shown in fig. S4, which is slightly lower than that in DMA maybe because of the absence of vibration stress]. The driving force for shape recovery produced by such a transformation can markedly surpass the creep resistance. Specifically, the nominal recovery stress of the Nitinol scaffold exceeds 70 MPa at 350°C, which is around four times higher than the plateau stress of the magnesium (~18 MPa) (Fig. 5B). As shown in Fig. 5E, the imposed deformation can almost be fully recovered by ~99% and by more than 60% for samples compressed to 4.5 and 10% strains, respectively, revealing a high potency for shape recovery. In addition, around one-fifth of the deformation can still be recovered even when the composite has been substantially deformed by a 40% strain. As shown in the inset, the three critical requirements for the achievement of this unique shape recovery behavior in the composite include (i) the heat-induced martensite-to-austenite phase transformation of Nitinol, (ii) the creep deformation of magnesium at lower stress, and (iii) an effective load transfer between the two phases enabled by the interpenetrating-phase architecture. It is also possible to partially recover the shape of the Mg-NiTi composite at ambient temperature owing to its elastic and viscoelastic characteristics. However, this effect becomes markedly less prominent as the applied deformation increases. The deformation in the Nitinol scaffold cannot be fully recovered by elasticity when the strain exceeds 2%, as manifested by the loading-unloading stress-strain curves of the scaffolds compressed to different strains shown in fig. S5.

The shape recovery behavior of the composite is additionally accompanied by some degree of restoration of its mechanical properties, specifically strength. As shown in Fig. 5F, the stress corresponding to 4% strain (relative to the sample's initial height) can retain ~90% of its original value in a composite sample, which has been deformed and recovered repeatedly by five times. The recovery potency in shape, as manifested by the ratio of recovered to total deformation, displays a decreasing trend with increasing cycles of deformation and recovery (inset). Nevertheless, the applied deformation can still be recovered by more than 60% after the fifth deformation cycle. This indicates a good stability for the recovery behavior of the Mg-NiTi composite in both shape and strength.

DISCUSSION

The strength and damping capacity at ambient to elevated temperatures are two of the most important mechanical properties of magnesium and magnesium alloys for applications involving lightweight structural materials. However, the simultaneous enhancement of these properties, specifically in terms of strengthening magnesium without compromising its damping capacity, still remains a key challenge (*5*–*11*). This is because the strength and damping capacity originate principally from two contradictive strategies—the respective obstruction and promotion of dislocation motion (*4*, *5*); accordingly, these properties are invariably mutually exclusive. In particular, magnesium-based composites strengthened by discrete reinforcements, e.g., particles, fibers, and whiskers, often exhibit decreased damping capacity and ductility than their unreinforced matrix materials (*13*–*15*). However, our success in attaining both high strength and good damping capacities in the current Mg-NiTi interpenetrating-phase composite can be attributed to the multiple designs of its chemical and architectural characteristics.

On the one hand, the Nitinol reinforcement exhibits markedly higher strengths than the magnesium matrix at ambient to elevated temperatures and can be notably work hardened during the large plastic deformation of its martensitic phase (fig. S1) (*16*). This endows the composite with a high apparent work-hardening ability to realize a higher strength. As the temperature rises, the Nitinol skeleton plays an increasing role in carrying load in the composite, as its strength is less sensitive to temperature (Nitinol displays an insignificant decrease in strength up to 400°C) (*29*). This acts to diminish any weakening effect in the Mg-NiTi composite caused by creep deformation of the magnesium matrix. In addition, the markedly higher melting point of Nitinol compared to magnesium offers a wide range of temperatures to conduct the infiltration process. The weak precipitates resulting from the limited reaction between magnesium melt and the Nitinol during infiltration, i.e., the Ti-rich interfacial phase and the Mg_2Ni phase at the grain boundaries of magnesium matrix, may serve as prime sites for microyielding and thus promote the damping capacities of the composite (*22*). It has been revealed that microdamage and even microcracks, which are preferentially formed at the precipitates in the current composite, could help absorb more mechanical energy by enabling new damping mechanisms such as the friction at the microcrack surfaces (*22*, *30*).

On the other hand, the 3D interpenetrating-phase architecture plays a key role in enhancing the mechanical properties, by retaining structural integrity and resisting the development of damage in the current Mg-NiTi composite. The bicontinuity of the Nitinol reinforcement and magnesium matrix is respectively beneficial for generating substantial strengthening and damping capacities in the composite by permitting effective stress transfer within each phase. The spread of damage, specifically from plastic deformation in the magnesium and cracking in the Nitinol, can be confined by the interlocking and partition between the two phases (Fig. 4). This leads to a controlled damaging process, which avoids catastrophic failure, and thereby engenders a high damage tolerance and energy absorption efficiency in the composite. The detrimental effects caused by easy precipitate fracture can also be mitigated by such means. In

contrast, the development of plastic damage throughout the magnesium matrix could result in global failure of composites with discrete reinforcements (*13*–*15*). In addition, the interpenetrating-phase architecture can act to relieve the stresses and exert constraint on the Nitinol reinforcement skeleton. This helps improve the mechanical stability and strength of the Nitinol structure, specifically as compared to traditional porous scaffolds, which commonly fail by the easy buckling of their struts (*12*, *14*). The bicontinuous nature of constituent phases and their interpenetration are also critical for the shape recovery process by promoting effective load delivery and enhancing the deformation compatibility between them.

To demonstrate that a combination of superior mechanical properties, i.e., strength, damping capacities, and energy absorption efficiency, has been achieved in our Mg-NiTi interpenetrating-phase composite, we provide a comparison in Fig. 6 with other materials with the strength represented using the maximum transmitted stress (*5*–*11*, *13*–*15*, *19*, *20*, *26*, *27*, *31*–*38*). The maximum transmitted stress and energy absorption efficiency, which are two basic parameters for evaluating the energy absorption performance of materials, are defined using the peak stress at the plateau stage and the area under the stress-strain curve before the steep stress rise, respectively (the detailed definition methods are illustrated in fig. S2) (*31*, *38*). It can be seen that our composite outperforms the majority of magnesium alloys, metal and polymer foams and microlattices, and other commonly used energy-absorbing materials, e.g., elastomers, plastics, and lead alloys, with respect to the combination of the efficiency and load-bearing ability for energy absorption (Fig. 6A). Specifically, the Mg-NiTi composite exhibits a stable plateau stage on the stress-strain curve, which is widespread in cellular materials but is rarely attainable in dense metals. Note that dense metals usually display continuously rising stress-strain curves, which are unfavorable for energy absorption applications, as the applied stress generally does not exceed the material's yield strength during energy absorption (*36*, *37*). This leads to a high-energy absorption efficiency in the composite, which surpasses the general ranges for magnesium, aluminum, and titanium alloys and is comparable to that of steels.

Among the magnesium-based alloys and composites, in general, relatively good damping capacities with internal friction more than 0.04 (for 0.1% strain amplitude with a frequency of 1 Hz at ambient temperature) can only be generated at low strength levels not exceeding 220 MPa (Fig. 6B). The distinct damping capacity with internal friction exceeding 0.08 in conjunction with a high strength higher than 320 MPa in the current composite breaks through the traditional benchmark of properties for magnesium-based materials. The properties of the Mg-NiTi composite also substantially exceed the strength, damping capacity, and energy absorption efficiency of simple mixtures of its constituents. Moreover, the material is capable of recovering its initial shape and strength to a large extent after deformation, simply by heat treatment, due to the martensite-to-austenite phase transformation in the Nitinol, which compensates for the low creep resistance of the magnesium matrix. The combination of the outstanding mechanical properties, i.e., strength, damping capacities, and energy absorption efficiency, with such shape-memory or even self-healing characteristics, endows this lightweight Mg-NiTi interpenetrating-phase composite with a broad range of potential applications, specifically for reducing vibrations and resisting impacts.

CONCLUSIONS

In summary, a new Mg-NiTi interpenetrating-phase composite has been developed by pressureless infiltration of a 3D printed reinforced scaffold of Nitinol with a magnesium melt. Mechanically, the composite exhibits an improved strength at ambient to elevated temperatures, exceeding that of a rule-of-mixtures estimate of its constituents, and displays excellent resistance to damage. These characteristics are accompanied by a synergetic enhancement of its damping capacity at differing strain amplitudes and a high-energy absorption efficiency, which are rarely attained in monolithic and

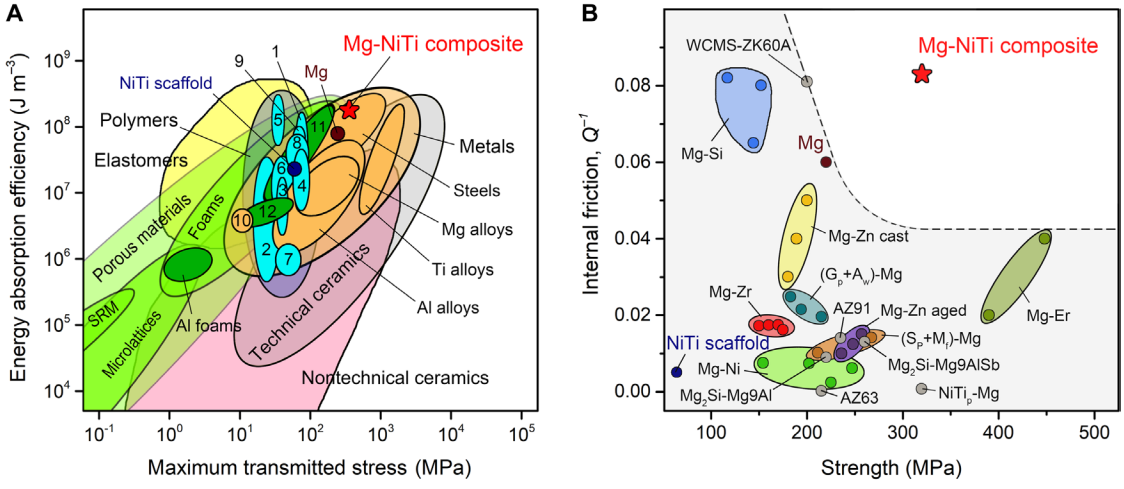

Fig. 6. Comparison of the properties of the Mg-NiTi composite with other materials (*5*–*11*, *13*–*15*, *19*, *20*, *26*, *27*, *31*–*38*). (**A**) Energy absorption per unit volume versus the maximum transmitted stress for the Mg-NiTi composite, magnesium alloys, and a wide range of other materials, specifically those commonly used for energy absorption (*19*, *20*, *26*, *27*, *31*, *34*, *35*, *37*, *38*). SRM, shape-reconfigurable materials. (**B**) Internal friction at 0.1% strain amplitude with a frequency of 1 Hz at ambient temperature along with the strength of the Mg-NiTi composite and other magnesium-based alloys and composites (*5*–*11*, *13*–*15*, *32*, *33*, *36*).

composite magnesium alloys. Moreover, both the initial shape and strength of composite can be largely recovered after deformation by heat treatment owing to the coupling of the martensite-to-austenite phase transformation in Nitinol with the low creep resistance of the magnesium matrix. Specifically, the Nitinol skeleton provides for a high work-hardening ability and offers the driving force for self-recovery of the composite; it additionally enables the infiltration process for fabrication. The bicontinuous interpenetrating-phase architecture plays a critical role in ensuring a potent strengthening effect by the Nitinol reinforcement while promoting good damping capacities by permitting effective load transfer. It also functions to resist the evolution of damage in the constituents throughout the microstructure, which promotes the composite's high-energy absorption efficiency and facilitates the recovery process. The unprecedented combination of mechanical properties in a magnesium-based material makes the composite a promising candidate for structural and biomedical applications, particularly in situations that require reduced vibrations and resistance to impacts. The temperature-responsive nature may even offer new promise for thermally reconfigurable or thermally strengthened structures. We anticipate that the current design concept and fabrication techniques could be extended to other alloy systems, e.g., W-Cu composites as high-voltage electrical contacts and heat sinks (*39*), for generating improved properties and functionalities.

MATERIALS AND METHODS

Architectural design

A stereolithographic 3D model with Voronoi tessellation of face-centered cubic polyhedra, termed rhombic dodecahedrons, was created for the porous Nitinol scaffold using the Pro/Engineer 5.0 software (Parametric Technology Corporation, USA). Such an architecture is frequently used in a wide range of natural materials, e.g., honeycombs, diamond, and garnet minerals, and has been intensively investigated in terms of its mechanical properties and mechanics, specifically for materials made by additive manufacturing (*23*, *24*, *26*, *27*). The scaffold was designed to contain 3 × 3 × 3 arrays of unit cells, with each cell having a dimension of 3.33 mm × 3.33 mm × 3.33 mm. The model was then sliced and processed using the commercial Materialise Magics 21.0 software (Materialise, Belgium) into layers with a thickness of 50 μm.

3D printing

Sequential printing of sliced layers was carried out by selective laser melting technique using a Realizer SLM 100 machine (Realizer GmbH, Germany) equipped with a Yb:YAG fiber laser. Nitinol powders with a median diameter of ~35 μm (AMC Powders Co., China) were used for printing. Before printing, the chamber was purged with high-purity argon gas until the oxygen content was lower than 0.1% to minimize oxidation. The substrate was preheated to 200°C to reduce residual stress, avoid cracking, and ensure a good dimensional accuracy of the printed scaffold (*23*, *40*). The layer thickness of the powders was set to be 50 μm, i.e., the same as that of the sliced layers in the digital model. The printing process was conducted using a laser power of 175 W and at a scanning speed of 750 mm/s. The scanning direction was rotated by 90° between layers.

Melt infiltration

Pressureless infiltration of the magnesium melt into the 3D printed Nitinol scaffold was performed in a high-purity graphite crucible at 800°C, i.e., some 150°C higher than the melting point of magnesium, for 10 min in flowing argon gas using a SRYL-2300/9 graphite resistance furnace (Jvjing Instrument, China), and then cooled in furnace. Before infiltration, the Nitinol scaffolds and magnesium blocks were ultrasonically cleaned in acetone to reduce contamination.

Microstructural characterization

The density of the infiltrated composite was measured using the Archimedes method. The phase constitution was examined by XRD using a Bruker D8 Advance x-ray diffractometer (Bruker AXS, Germany) with Co-Kα radiation. Microzone XRD analysis was also conducted using a Bruker D8 Discover x-ray microdiffractometer (Bruker AXS, Germany) with Co-Kα radiation at an accelerating voltage of 40 kV using an x-ray beam with 0.5 mm in diameter. SEM imaging was performed using a LEO Supra-35 field-emission SEM (LEO, Germany) operating at an accelerating voltage of 20 kV. EDS measurement was carried out using an Oxford Model 7426 spectrometer (Oxford Instruments, UK) equipped with the microscope.

XRT imaging

The 3D architecture of the Mg-NiTi composite was characterized by XRT imaging using an Xradia Versa XRM-500 3D x-ray microscope (Xradia, USA) operating at an accelerating voltage of 80 kV. The sample was rotated by 360° around the normal axis of the x-ray source and detector and imaged every 0.225° to generate 1600 slices of 2D projections. The 3D volume renderings were reconstructed by inversing these projections based on the Fourier back-projection algorithm. The spatial resolution of the 3D image was ~12 μm per pixel. Images were processed and analyzed using the Avizo Fire 7.1 software (Visualization Sciences Group, France).

Mechanical testing

Samples for mechanical testing were ground and polished to dimensions of ~9 mm × 9 mm in cross section and ~8 mm in height. Quasi-static uniaxial compression tests were performed at ambient temperature, 200°C, and 350°C with a fixed strain rate of 10^{-3} s^{-1} using an Instron 5982 testing system (Instron Corp., USA). For cyclic compression, a sample was loaded and unloaded repeatedly at a fixed strain rate of 10^{-3} s^{-1} to create a constant increase in stress of ~10 MPa at each cycle until reaching the plateau stage on the stress-strain curve for monotonic compression. A series of 3D printed Nitinol scaffolds without infiltration were compressed to different strains and then unloaded at the same strain rate. DMA was performed at ambient temperature up to 350°C, on samples with the same dimension as that used for the compression testing, using a Gabo Eplexor 4000N dynamic thermomechanical analyzer (NETZSCH, Germany). This was conducted in compression mode by applying a sinusoidal cyclic load at a frequency of 1 Hz and with dynamic strain amplitudes of 0.001, 0.01, and 0.1%, respectively.

Shape recovery measurement

The shape recovery process of the deformed Mg-NiTi composites was accomplished by treating them at 350°C for 3 hours. Samples with differing degrees of deformation, i.e., by compression to roughly 4.5, 7.5, 10, 15, 20, 25, 30, and 40% strain on the stress-strain curves, were recovered and gauged before and after the recovery treatment. In addition, a sample was repeatedly compressed at ambient temperature to a strain of ~4.5% of its original height, unloaded, and then recovered via heat treatment by up to five times to examine the

potency and stability of the recovery behavior of composite in terms of the shape and strength of the test sample. The thermal behavior of the Nitinol scaffold was characterized by DSC analysis using a Q20 calorimeter (TA Instruments, DE) with a heating rate of 10 K/min.

SUPPLEMENTARY MATERIALS

Supplementary material for this article is available at http://advances.sciencemag.org/cgi/content/full/6/19/eaba5581/DC1

REFERENCES AND NOTES

1. T. M. Pollock, Weight loss with magnesium alloys. *Science* **328**, 986–987 (2010).
2. S. R. Agnew, Wrought magnesium: A 21st century outlook. *JOM* **56**, 20–21 (2004).
3. K. Sugimoto, K. Niiya, T. Okamoto, K. Kishitake, A study of damping capacity in magnesium alloys. *Trans. JIM* **18**, 277–288 (1977).
4. Y. Cui, Y. Li, S. Sun, H. Bian, H. Huang, Z. Wang, Y. Koizumi, A. Chiba, Enhanced damping capacity of magnesium alloys by tensile twin boundaries. *Scripta Mater.* **101**, 8–11 (2015).
5. R. Schaller, Metal matrix composites, a smart choice for high damping materials. *J. Alloys Compd.* **355**, 131–135 (2003).
6. H. Feng, H. Liu, H. Cao, Y. Yang, Y. Xu, J. Guan, Effect of precipitates on mechanical and damping properties of Mg-Zn-Y-Nd alloys. *Mater. Sci. Eng. A* **639**, 1–7 (2015).
7. D. Wan, J. Wang, G. Yang, A study of the effect of Y on the mechanical properties, damping properties of high damping Mg-0.6%Zr based alloys. *Mater. Sci. Eng. A* **517**, 114–117 (2009).
8. C. Xu, J. Zhang, S. Liu, Y. Jing, Y. Jiao, L. Xu, L. Zhang, F. Jiang, M. Zhang, R. Wu, Microstructure, mechanical and damping properties of Mg-Er-Gd-Zn alloy reinforced with stacking faults. *Mater. Des.* **79**, 53–59 (2015).
9. J. Wang, Z. Wu, S. Gao, R. Lu, D. Qin, W. Yang, F. Pan, Optimization of mechanical and damping properties of Mg-0.6 Zr alloy by different extrusion processing. *J. Magnes. Alloys* **3**, 79–85 (2015).
10. Q. Li, J. Li, G. He, Compressive properties and damping capacities of magnesium reinforced with continuous steel wire. *Mater. Sci. Eng. A* **680**, 92–96 (2017).
11. X. S. Hu, K. Wu, M. Y. Zheng, W. M. Gan, X. J. Wang, Low frequency damping capacities and mechanical properties of Mg-Si alloys. *Mater. Sci. Eng. A* **452–453**, 374–379 (2007).
12. R. O. Ritchie, The conflicts between strength and toughness. *Nat. Mater.* **10**, 817–822 (2011).
13. J. Gu, X. Zhang, M. Gu, Mechanical properties and damping capacity of (SiC_p + $Al_2O_3{\cdot}SiO_{2f}$)/Mg hybrid metal matrix composite. *J. Alloys Compd.* **385**, 104–108 (2004).
14. S. Seshan, M. Jayamathy, S. V. Kailas, T. S. Srivatsan, The tensile behavior of two magnesium alloys reinforced with silicon carbide particulates. *Mater. Sci. Eng. A* **363**, 345–351 (2003).
15. S. Ugandhar, M. Gupta, S. K. Sinha, Enhancing strength and ductility of Mg/SiC composites using recrystallization heat treatment. *Compos. Struct.* **72**, 266–272 (2006).
16. J. Van Humbeeck, Damping capacity of thermoelastic martensite in shape memory alloys. *J. Alloys Compd.* **355**, 58–64 (2003).
17. K. Milička, J. Čadek, P. Ryš, High temperature creep mechanisms in magnesium. *Acta Metall.* **18**, 1071–1082 (1970).
18. D. R. Clarke, Interpenetrating phase composites. *J. Am. Ceram. Soc.* **75**, 739–759 (1992).
19. L. Wang, J. Lau, E. L. Thomas, M. C. Boyce, Co-continuous composite materials for stiffness, strength, and energy dissipation. *Adv. Mater.* **23**, 1524–1529 (2011).
20. O. Al-Ketan, R. K. A. Al-Rub, R. Rowshan, Mechanical properties of a new type of architected interpenetrating phase composite materials. *Adv. Mater. Technol.* **2**, 1600235 (2017).
21. G. Parande, V. Manakari, S. Wakeel, M. S. Kujur, M. Gupta, Enhancing mechanical response of monolithic magnesium using nano-NiTi (Nitinol) particles. *Metals* **8**, 1014 (2018).
22. I. S. Golovin, H. R. Sinning, J. Göken, W. Riehemann, Amplitude dependent damping of some metallic foams. *Solid State Phenom.* **89**, 267–272 (2003).
23. A. Vyatskikh, S. Delalande, A. Kudo, X. Zhang, C. M. Portela, J. R. Greer, Additive manufacturing of 3D nano-architected metals. *Nat. Commun.* **9**, 593 (2018).
24. D. D. Gu, W. Meiners, K. Wissenbach, R. Poprawe, Laser additive manufacturing of metallic components: Materials, processes and mechanisms. *Int. Mater. Rev.* **57**, 133–164 (2012).
25. N. Read, W. Wang, K. Essa, M. M. Attallah, Selective laser melting of AlSi10Mg alloy: Process optimization and mechanical properties development. *Mater. Des.* **65**, 417–424 (2015).
26. S. Babaee, B. H. Jahromi, A. Ajdari, H. Nayeb-Hashemi, A. Vaziri, Mechanical properties of open-cell rhombic dodecahedron cellular structures. *Acta Mater.* **60**, 2873–2885 (2012).
27. T. A. Schaedler, A. J. Jacobsen, A. Torrents, A. E. Sorensen, J. Lian, J. R. Greer, L. Valdevit, W. B. Carter, Ultralight metallic microlattices. *Science* **334**, 962–965 (2011).
28. V. C. Shunmugasamy, B. Mansoor, N. Gupta, Cellular magnesium matrix foam composites for mechanical damping applications. *JOM* **68**, 279–287 (2016).
29. R. R. Adharapurapu, F. Jiang, K. S. Vecchio, G. T. Gray III, Response of NiTi shape memory alloy at high strain rate: A systematic investigation of temperature effects on tension-compression asymmetry. *Acta Mater.* **54**, 4609–4620 (2006).
30. J. Göken, W. Riehemann, Damping behavior of AZ91 magnesium alloy with cracks. *Mater. Sci. Eng. A* **370**, 417–421 (2004).
31. T. A. Schaedler, C. J. Ro, A. E. Sorensen, Z. Eckel, S. S. Yang, W. B. Carter, A. J. Jacobsen, Designing metallic microlattices for energy absorber applications. *Adv. Eng. Mater.* **16**, 276–283 (2014).
32. I. D. Choi, D. M. Kim, K. M. Cho, I. M. Park, Damping and mechanical properties of (graphite + $9Al_2O_3{\cdot}2B_2O_3$)/Mg metal matrix composites. *Mater. Sci. Forum* **449-452**, 657–660 (2004).
33. S. Wakeel, V. Manakari, G. Parande, M. S. Kujur, A. A. Khan, M. Gupta, Synthesis and mechanical response of NiTi SMA nanoparticle reinforced Mg composites synthesized through microwave sintering process. *Mater. Today. Proc.* **5**, 28203–28210 (2018).
34. X. N. Zhang, R. J. Wu, Damping capacity of pure Mg metal matrix composites. *Key Eng. Mater.* **249**, 217–222 (2003).
35. M. F. Ashby, *Materials Section in Mechanical Design* (Pergamon Press, Oxford, ed. 3, 2005).
36. X.-Q. Xie, T.-X. Fan, D. Zhang, R.-J. Wu, Increasing the mechanical properties of high damping wood ceramics by infiltration with a magnesium alloy. *Compos. Sci. Technol.* **62**, 1341–1346 (2002).
37. B. Haghpanah, L. Salari-Sharif, P. Pourrajab, J. Hopkins, L. Valdevit, Multistable shape-reconfigurable architected materials. *Adv. Mater.* **28**, 7915–7920 (2016).
38. M. Avalle, G. Belingardi, R. Montanini, Characterization of polymeric structural foams under compressive impact loading by means of energy-absorption diagram. *Int. J. Impact Eng.* **25**, 455–472 (2001).
39. M. Calvo, A. E. Jakus, R. N. Shah, R. Spolenak, D. C. Dunand, Microstructure and processing of 3D printed tungsten microlattices and infiltrated W-Cu composites. *Adv. Eng. Mater.* **20**, 1800354 (2018).
40. R. Mertens, B. Vrancken, N. Holmstock, Y. Kinds, J.-P. Kruth, J. Van Humbeeck, Influence of powder bed preheating on microstructure and mechanical properties of H13 tool steel SLM parts. *Phys. Proc.* **83**, 882–890 (2016).

Acknowledgments

Funding: The authors are grateful for the financial support by the National Natural Science Foundation of China under grant nos. 51871216 and 51331007 (for Z.L. and Z.Z.), the LiaoNing Revitalization Talents Program (for Z.L. and Z.Z.), the Key Research Program of Frontier Sciences CAS under grant no. QYZDJ-SSW-JSC031 (for S.L. and R.Y.), the Opening Project of Jiangsu Province Key Laboratory of High-End Structural Materials under grant no. hsm1801 (for Z.L.), and the Multi-University Research Initiative under grant no. AFOSR-FA9550-15-1-0009 from the Air Force Office of Scientific Research (for R.O.R.). **Author contributions:** Z.L. and S.L. designed the research. M.Z., J.Z., and G.T. fabricated the Mg-NiTi composite. S.L. and R.Y. carried out 3D printing. M.Z. and D.J. characterized the microstructures. M.Z., Q.Y., and W.Z. measured the mechanical properties. All the authors analyzed and discussed the data. M.Z. and Z.L. wrote the initial paper. Z.Z., R.Y., and R.O.R. revised the paper. **Competing interests:** The authors declare that they have no competing interests. **Data and materials availability:** All data needed to evaluate the conclusions in the paper are present in the paper and/or the Supplementary Materials. Additional data related to this paper may be requested from the authors.

Submitted 12 December 2019
Accepted 24 February 2020
Published 8 May 2020
10.1126/sciadv.aba5581

Citation: M. Zhang, Q. Yu, Z. Liu, J. Zhang, G. Tan, D. Jiao, W. Zhu, S. Li, Z. Zhang, R. Yang, R. O. Ritchie, 3D printed Mg-NiTi interpenetrating-phase composites with high strength, damping capacity, and energy absorption efficiency. *Sci. Adv.* **6**, eaba5581 (2020).